Received: 9 June 2017 | Accepted: 23 August 2017

DOI: 10.1002/asna.201713384

ORIGINAL ARTICLE

Astronomische Nachrichten

The contribution of kinetic helicity to turbulent magnetic diffusivity

A. Brandenburg[1,2,3,4,*] | **J. Schober**[3,5] | **I. Rogachevskii**[6,1,3]

[1]Laboratory for Atmospheric and Space Physics, University of Colorado, Boulder, Colorado
[2]JILA and Department of Astrophysical and Planetary Sciences, University of Colorado, Boulder, Colorado
[3]Nordita, KTH Royal Institute of Technology and Stockholm University, Stockholm, Sweden
[4]Department of Astronomy, AlbaNova University Center, Stockholm University, Stockholm, Sweden
[5]Laboratoire d'Astrophysique, EPFL, CH-1290 Sauverny, Switzerland
[6]Department of Mechanical Engineering, Ben-Gurion University of the Negev, Beer-Sheva, Israel

***Correspondence**
A. Brandenburg, Nordita, KTH Royal Institute of Technology and Stockholm University, 10691 Stockholm, Sweden.
Email: brandenb@nordita.org

Funding Information
National Science Foundation, AST1615100. Research Council of Norway, FRINATEK 231444. European Union's Horizon 2020 research and innovation programme under the Marie Skłodowska-Curie grant 665667. National Science Foundation, CNS-0821794. University of Colorado Boulder. University of Colorado Denver. National Center for Atmospheric Research.

Using numerical simulations of forced turbulence with and without mean kinetic helicity, we show that for magnetic Reynolds numbers larger than unity, that is, beyond the regime of quasilinear theory, the turbulent magnetic diffusivity attains an additional negative contribution that is quadratic in the kinetic helicity. In particular, for large magnetic Reynolds numbers, the turbulent magnetic diffusivity without helicity is about twice the value with helicity. Such a contribution was not previously anticipated, but, as we discuss, it turns out to be important when accurate estimates of the turbulent magnetic diffusivity are needed.

KEYWORDS
magnetic fields – magnetohydrodynamics (MHD) – turbulence

1 | INTRODUCTION

Large-scale magnetic fields in the turbulent convection zones of stars or in supernova-driven turbulence of the interstellar medium of galaxies evolve according to the equations of mean-field electrodynamics and, in particular, the mean-field induction equation. This equation is similar to the original induction equation for the actual magnetic field, which includes the fluctuations around the mean magnetic field. The presence of turbulence leads to enhanced effective magnetic diffusion, which is often orders of magnitude larger than the microphysical value, although this is usually not the case in numerical simulations and no restriction concerning this ratio will be made in this paper. If the velocity field is helical, there is, in addition to ordinary turbulent diffusion, also the α effect, which can destabilize an initially weak large-scale magnetic field and lead to its exponential growth.

Mathematically, the evolution of the mean magnetic field $\overline{\mathbf{B}}$ is described by the equation

$$\frac{\partial \overline{\mathbf{B}}}{\partial t} = \boldsymbol{\nabla} \times [\alpha \overline{\mathbf{B}} - (\eta_t + \eta)\mu_0 \overline{\mathbf{J}}], \tag{1}$$

where $\overline{\mathbf{J}} = \boldsymbol{\nabla} \times \overline{\mathbf{B}}/\mu_0$ is the mean current density, μ_0 is the vacuum permeability, and η is the microphysical magnetic diffusivity, and overbars denote spatial averaging, which we will later specify to be horizontal averaging over two spatial coordinates x and y. For the purpose of this discussion, and throughout this paper, we assume the turbulence to be isotropic; otherwise, α and η_t would have to be replaced by tensors.

The relative importance of turbulent diffusion to microphysical diffusion is measured by the magnetic Reynolds number

$$R_m = u_{rms}/\eta k_f, \tag{2}$$

where u_{rms} is the root-mean-squared (rms) velocity of the turbulence, and k_f is the wavenumber of the energy-carrying eddies. The magnetic diffusivity and the α effect are inversely proportional to the electric conductivity in the low conductivity limit, that is, $R_m \ll 1$, so we have (Krause & Rädler 1980)

$$\eta_t = -\frac{1}{3\eta}(\overline{\boldsymbol{\psi}^2} - \overline{\phi^2}) \quad \text{and} \quad \alpha = -\frac{1}{3\eta}\overline{\boldsymbol{\psi} \cdot \mathbf{u}}, \tag{3}$$

where $\mathbf{u} = \nabla \times \psi + \nabla\phi$ is the turbulent velocity expressed in terms of a vector potential ψ and a scalar potential ϕ. In

the following, we perform averaging over two coordinate directions.

One often considers the limiting case of incompressible turbulence, so $\phi=0$ and $\overline{\boldsymbol{\psi}^2}=\overline{\mathbf{u}^2}/k_\mathrm{f}^2$, and $\overline{\boldsymbol{\psi}\cdot\mathbf{u}}=\overline{\boldsymbol{\omega}\cdot\mathbf{u}}/k_\mathrm{f}^2$, where $\boldsymbol{\omega}=\nabla\times\mathbf{u}$ is the vorticity. In that case, we can write

$$\eta_\mathrm{t}=\frac{1}{3}\tau\overline{\mathbf{u}^2}\qquad\text{and}\qquad\alpha=-\frac{1}{3}\tau\overline{\boldsymbol{\omega}\cdot\mathbf{u}} \tag{4}$$

with

$$\tau=(\eta k_\mathrm{f}^2)^{-1} \tag{5}$$

being the microphysical magnetic diffusion time based on the wavenumber k_f. We reiterate that this expression applies only to isotropic conditions. Indeed, simple anisotropic flows can be constructed, where $\overline{\boldsymbol{\omega}\cdot\mathbf{u}}=0$ but $\overline{\boldsymbol{\psi}\cdot\mathbf{u}}\neq0$, and so those do yield an α effect (Rädler & Brandenburg 2003). Furthermore, in the compressible case, there is a negative contribution to η_t, so that it can even become negative, as has been demonstrated for deterministic flows by Rädler et al. (2011).

By contrast, in the high-conductivity limit, $R_\mathrm{m}\gg1$, Equation (4) still applies (Krause & Rädler 1980), but now with

$$\tau\approx(u_\mathrm{rms}k_\mathrm{f})^{-1}\qquad(R_\mathrm{m}\gg1) \tag{6}$$

being the correlation time. This was also confirmed numerically using the test-field method (Sur et al. 2008), although our new results discussed below will show a slight twist to the R_m dependence of their result.

Equation (4) is also motivated by symmetry arguments. In particular, since α is a pseudoscalar, it is clear that in the present case, where the only pseudoscalar in the system is $\overline{\boldsymbol{\omega}\cdot\mathbf{u}}$, there can be no other contribution to α. This is, however, not the case for η_t, which is just an ordinary scalar. Thus, in the present case, there may well be an additional contribution proportional to $(\overline{\boldsymbol{\omega}\cdot\mathbf{u}})^2$, for example. The purpose of this paper is to show that this is indeed the case.

A particularly useful diagnostics is the ratio η_t/α, because it is expected to be independent of τ and equal to $\overline{\mathbf{u}^2}/\overline{\boldsymbol{\omega}\cdot\mathbf{u}}$ in the limit of small magnetic Reynolds numbers, where Equation (4) is obeyed exactly. In this paper, we shall confirm that this is indeed the case when $R_\mathrm{m}\ll1$, but we find a departure from this simple result as R_m is increased. We shall use the test-field method (Schrinner et al. 2005, 2007), which has been highly successful in measuring turbulent transport coefficients in isotropic turbulence (Brandenburg et al. 2008b; Sur et al. 2008), shear flow turbulence (Brandenburg 2005; Brandenburg et al. 2008a; Gressel 2010; Gressel et al. 2008; Madarassy & Brandenburg 2010), cosmic ray driven turbulence (Rogachevskii et al. 2012), and magnetically quenched turbulence (Brandenburg et al. 2008c; Karak et al. 2014).

2 | TEST-FIELD METHOD IN TURBULENCE SIMULATIONS

As in a number of previous cases (e.g., Brandenburg 2001), we reconsider isotropically forced turbulence either with or without helicity using an isothermal equation of state. Since the magnetic field is assumed to be weak, there is no backreaction of the magnetic field on the flow. Furthermore, instead of solving for the magnetic field, we just solve for the fluctuations of the magnetic field that arise from a set of given test fields. This equation is given by

$$\frac{\partial\mathbf{b}^\mathrm{T}}{\partial t}=\boldsymbol{\nabla}\times(\mathbf{u}\times\overline{\mathbf{B}}^\mathrm{T}+\overline{\mathbf{U}}\times\mathbf{b}^\mathrm{T}+\mathbf{u}\times\mathbf{b}^\mathrm{T}-\overline{\mathbf{u}\times\mathbf{b}^\mathrm{T}})+\eta\nabla^2\mathbf{b}^\mathrm{T}. \tag{7}$$

Here, $\overline{\mathbf{U}}+\mathbf{u}\equiv\mathbf{U}$ is the time-dependent flow, which we take to be the solution to the momentum and continuity equations with constant sound speed c_s, a random forcing function $\mathbf{f}$, density ρ, and the traceless rate of strain tensor $\mathsf{S}_{ij}=\frac{1}{2}(U_{i,j}+U_{j,i})-\frac{1}{3}\delta_{ij}\boldsymbol{\nabla}\cdot\mathbf{U}$ (commas denote partial differentiation),

$$\frac{\partial\mathbf{U}}{\partial t}=-\mathbf{U}\cdot\boldsymbol{\nabla}\mathbf{U}-c_\mathrm{s}^2\boldsymbol{\nabla}\ln\rho+\frac{1}{\rho}\boldsymbol{\nabla}\cdot(2\nu\rho\mathbf{S})+\mathbf{f}, \tag{8}$$

$$\frac{\partial\ln\rho}{\partial t}=-\mathbf{U}\cdot\boldsymbol{\nabla}\ln\rho-\boldsymbol{\nabla}\cdot\mathbf{U}. \tag{9}$$

The following four test fields, $\overline{\mathbf{B}}^\mathrm{T}$, are used:

$$\begin{pmatrix}\cos k_1z\\0\\0\end{pmatrix},\begin{pmatrix}\sin k_1z\\0\\0\end{pmatrix},\begin{pmatrix}0\\\cos k_1z\\0\end{pmatrix},\begin{pmatrix}0\\\sin k_1z\\0\end{pmatrix}. \tag{10}$$

For each $\overline{\mathbf{B}}^\mathrm{T}$, the solutions $\mathbf{b}^\mathrm{T}$ allow us to compute the mean electromotive force, $\overline{\boldsymbol{\mathcal{E}}}^\mathrm{T}=\overline{\mathbf{u}\times\mathbf{b}^\mathrm{T}}$, and relate it to $\overline{\mathbf{B}}^\mathrm{T}$ and $\mu_0\overline{\mathbf{J}}^\mathrm{T}\equiv\boldsymbol{\nabla}\times\overline{\mathbf{B}}^\mathrm{T}$ via

$$\overline{\mathcal{E}}_i^\mathrm{T}=\alpha_{ij}\overline{B}_j^\mathrm{T}-\eta_{ij}\mu_0\overline{J}_j^\mathrm{T}. \tag{11}$$

The four independent test fields constitute eight scalar equations for the x and y components of $\overline{\boldsymbol{\mathcal{E}}}_i^\mathrm{T}$ with $i=1$ and 2, which can be solved for the eight unknown relevant components of α_{ij} and η_{ij} with $i,j=1,2$. The $i=3$ component does not enter because we use averaging over x and y, so $\overline{B}_3=\mathrm{const}=0$ owing to $\boldsymbol{\nabla}\cdot\overline{\mathbf{B}}=0$ and the absence of a uniform imposed field.

For isotropically forced turbulence, we expect $\alpha_{12}=\alpha_{21}=\eta_{12}=\eta_{21}=0$, $\alpha_{11}=\alpha_{22}=\alpha$, and $\eta_{11}=\eta_{22}=\eta_\mathrm{t}$. This is, however, only true in a statistical sense, and since α and η_t are still functions of z and t, we must average over these two coordinates; so we compute

$$\alpha=\frac{1}{2}\langle\alpha_{11}+\alpha_{22}\rangle_{zt},\qquad\eta_\mathrm{t}=\frac{1}{2}\langle\eta_{11}+\eta_{22}\rangle_{zt}, \tag{12}$$

where $\langle\cdot\rangle_{zt}$ denotes averaging over z and t.

We use the forcing function $\mathbf{f}$ which consists of random, white-in-time, plane waves with a certain average wavenumber k_f (Brandenburg 2001):

$$\mathbf{f}(\mathbf{x},t)=\mathrm{Re}\{N\tilde{\boldsymbol{f}}(\mathbf{k},t)\exp[\mathrm{i}\mathbf{k}\cdot\mathbf{x}+\mathrm{i}\phi]\}, \tag{13}$$

where $\mathbf{x}$ is the position vector. We choose $N=f_0\sqrt{c_\mathrm{s}^3|\mathbf{k}|}$, where f_0 is a nondimensional forcing amplitude. At each timestep, we select randomly the phase $-\pi<\phi\leq\pi$ and the wavevector $\mathbf{k}$ from many possible discrete wavevectors in

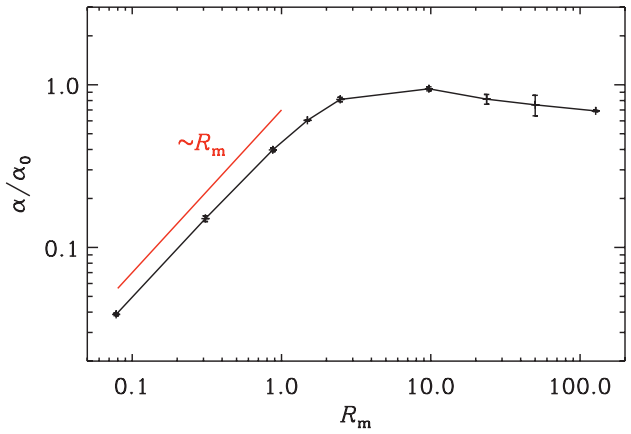

FIGURE 1 Dependence of α on R_m for the models with maximum helicity

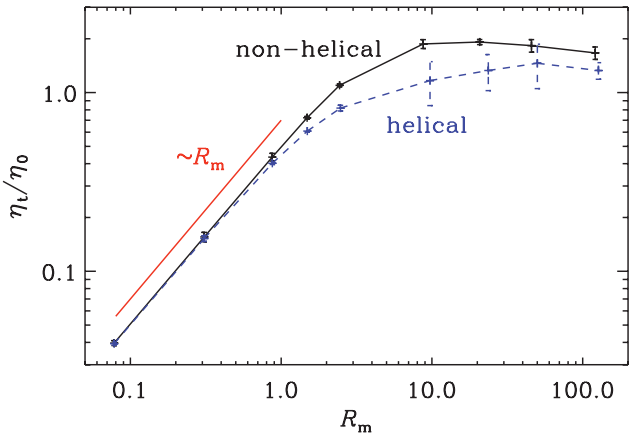

FIGURE 2 Dependence of η_t on R_m for models with maximum helicity (dashed blue) and with zero helicity (solid black)

a certain range around a given value of k_f. The Fourier amplitudes

$$\tilde{f}(\mathbf{k}) = \mathsf{R} \cdot \tilde{f}(\mathbf{k})^{(\mathrm{nohel})} \quad \text{with} \quad \mathsf{R}_{ij} = \frac{\delta_{ij} - \mathrm{i}\sigma\varepsilon_{ijk}\hat{k}}{\sqrt{1+\sigma^2}}, \tag{14}$$

where the parameter σ characterizes the fractional helicity of $\mathbf{f}$, and

$$\tilde{f}(\mathbf{k})^{(\mathrm{nohel})} = (\mathbf{k} \times \hat{\mathbf{e}})/\sqrt{\mathbf{k}^2 - (\mathbf{k} \cdot \hat{\mathbf{e}})^2} \tag{15}$$

is a nonhelical forcing function. Here, $\hat{\mathbf{e}}$ is an arbitrary unit vector not aligned with $\mathbf{k}$; $\hat{\mathbf{k}}$ is the unit vector along $\mathbf{k}$; and $|\tilde{f}|^2 = 1$.

We will consider both $\sigma = 0$ and $\sigma = 1$, corresponding to nonhelical and maximally helical cases. We vary R_m, defined in Equation (2), by changing η while keeping $\nu = \eta$ in all cases. We use the Pencil Code[1] with a numerical resolution of up to 288^3 mesh points in the case with $R_m \approx 120$, which is the largest value considered here.

3 | RESULTS

3.1 | Dependence of α and η_t on $\mathbf{R_m}$

As theoretically expected (Krause & Rädler 1980; Moffatt 1978) and previously demonstrated using the test-field method (Sur et al. 2008), α and η increase linearly with R_m for $R_m < 1$; see Figures 1 and 2 for nonhelical and helical cases. Here, the error bars have been evaluated as the maximum departure from the averages for any one-third of the full time series. In the helical case, both α and η saturate around unity, but in the nonhelical case, η overshoots the helical value by almost a factor of two; see Figure 2.

3.2 | Ratio of α to η_t

In Figure 3 we plot the ratio η_t/α, normalized by η_{t0}/α_0, where $\alpha_0 = -u_{rms}/3$ and $\eta_{t0} = u_{rms}/3k_f$. The minus sign in our expression for α_0 takes into account that we are forcing with positive helicity, which then leads to a negative α effect (Krause & Rädler 1980; Moffatt 1978). For small values of R_m, this ratio is unity, but it reaches a value of ~ 2 when $R_m \approx 50$.

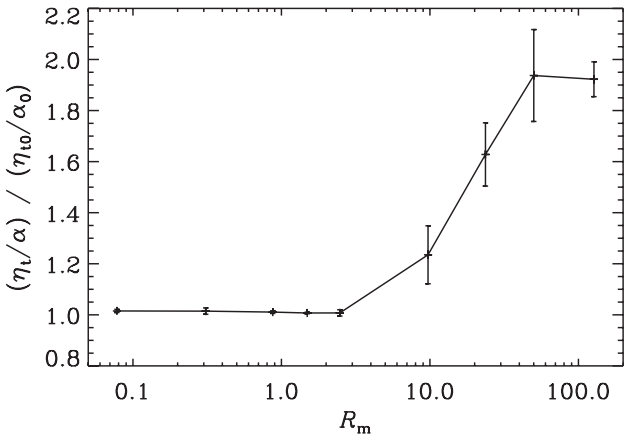

FIGURE 3 Ratio of η_t/α

3.3 | Difference between nonhelical and helical cases

It turns out that the difference between η_t in the nonhelical and helical cases increases quadratically in R_m; see Figure 4. This shows, first of all, that the difference vanishes for small R_m, but it also suggests that there is a correction to η_t due to the presence of helicity that is not captured by the second-order correlation approximation, which is exact for $R_m \ll 1$. It should be possible, however, to capture this effect of helicity on η_t using a higher order approximation, which has not yet been attempted, however.

3.4 | Relation to earlier results

A similar situation has been encountered previously in the case of the Galloway–Proctor flow (Galloway & Proctor 1992), where, in addition to an α effect and turbulent diffusion, also a turbulent pumping effect was found (Courvoisier et al. 2006). This result was not obtained under the second-order correlation approximation (Rädler & Brandenburg 2009). Using the test-field method, they showed, however, that the value of γ, which quantifies the

[1] https://github.com/pencil-code

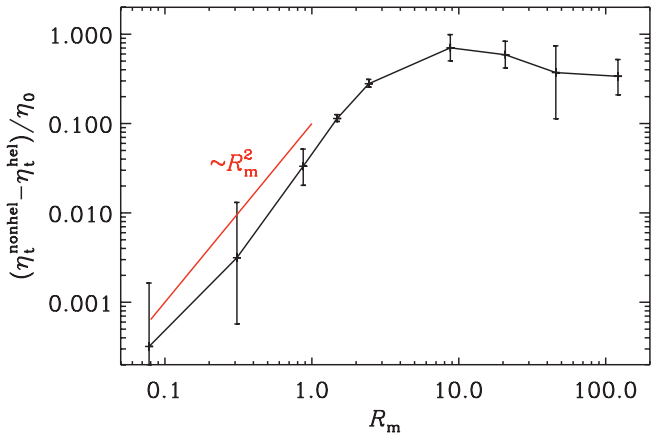

FIGURE 4 R_m dependence of the difference between η_t for models with zero helicity and maximum helicity

turbulent pumping velocity, does indeed vanish for $R_m \ll 1$, but it was found to increase with R_m as $R_m{}^5$; see Rädler & Brandenburg (2009), who interpreted this as a higher order effect that should be possible to capture with a sixth-order approximation. Our present result therefore suggests that the difference between nonhelical and helical cases can also be described as a result of a higher order approximation, which, in this case, would be a fourth-order approximation. It should also be possible to obtain this result via a path-integral approach for turbulence with finite but small correlation time, as in Kleeorin et al. (2002), but this is the subject of a separate study.

4 | CONCLUSIONS

Our present results have demonstrated that, at least for intermediate values of R_m in the range between 1 and 120, there is a contribution to the usual expression for the turbulent magnetic diffusivity $\eta_t = \tau\overline{\mathbf{u}^2}/3$ that depends on $(\overline{\boldsymbol{\omega}\cdot\mathbf{u}})^2$. This is somewhat surprising in the sense that such a result had not previously been reported, but it is fully compatible with all known constraints: no correction for $R_m \ll 1$ and no dependence on the sign of $\overline{\boldsymbol{\omega}\cdot\mathbf{u}}$. On the other hand, our results may still be compatible with the τ approximation in the high-conductivity limit if the difference between the turbulent diffusivity in the nonhelical and helical cases vanishes for $R_m \to \infty$. However, our numerical results do not clearly confirm this because our largest value of R_m was only $\sim$120.

There is a practically relevant application to this phenomenon, at least in the case of forced turbulence, where its effect on the large-scale magnetic field evolution can now be quantified to high accuracy. A factor of nearly two in the value of η_t is clearly beyond the acceptable accuracy for this case. This was noticed in recent studies of the α effect and turbulent diffusion in the presence of the chiral magnetic effect (Schober et al. 2017). Our present result therefore removes an otherwise noticeable discrepancy relative to the theoretical predictions. Future applications hinge obviously on the overall accuracy of analytic approximations to particular circumstances. In most cases, naturally driven flow turbulence will be anisotropic, so we expect more complicated tensorial results for turbulent diffusion.

ACKNOWLEDGMENTS

Support through the National Science Foundation (grant AST1615100), and the Research Council of Norway (FRINATEK grant 231444), are gratefully acknowledged. This project has received funding from the European Union's Horizon 2020 research and innovation programme under the Marie Skłodowska-Curie grant 665667. We acknowledge the allocation of computing resources provided by the Swedish National Allocations Committee at the Center for Parallel Computers at the Royal Institute of Technology in Stockholm. This work utilized the Janus supercomputer, which is supported by the National Science Foundation (award number CNS-0821794), the University of Colorado Boulder, the University of Colorado Denver, and the National Center for Atmospheric Research. The Janus supercomputer is operated by the University of Colorado, Boulder.

REFERENCES

Brandenburg, A. 2001, *ApJ*, *550*, 824.
Brandenburg, A. 2005, *Astron. Nachr.*, *326*, 787.
Brandenburg, A., Rädler, K.-H., Rheinhardt, M., & Käpylä, P. J. 2008a, *ApJ*, *676*, 740.
Brandenburg, A., Rädler, K.-H., & Schrinner, M. 2008b, *A&A*, *482*, 739.
Brandenburg, A., Rädler, K.-H., Rheinhardt, M., & Subramanian, K. 2008c, *ApJ*, *687*, L49.
Courvoisier, A., Hughes, D. W., & Tobias, S. M. 2006, *Phys. Rev. Lett.*, *96*, 034503.
Galloway, D. J., & Proctor, M. R. E. 1992, *Nature*, *356*, 691.
Gressel, O. 2010, *MNRAS*, *405*, 41.
Gressel, O., Ziegler, U., Elstner, D., & Rüdiger, G. 2008, *Astron. Nachr.*, *329*, 619.
Karak, B. B., Rheinhardt, M., Brandenburg, A., et al. 2014, *ApJ*, *795*, 16.
Krause, F., & Rädler, K.-H. 1980, *Mean-field Magnetohydrodynamics and Dynamo Theory*, Pergamon Press (Oxford).
Kleeorin, N., Rogachevskii, I., & Sokoloff, D. 2002, *Phys. Rev. E*, *65*, 036303.
Madarassy, E. J. M., & Brandenburg, A. 2010, *Phys. Rev. E*, *82*, 016304.
Moffatt, H. K. 1978, *Magnetic Field Generation in Electrically Conducting Fluids*, Cambridge University Press (Cambridge).
Rädler, K.-H., & Brandenburg, A. 2003, *Phys. Rev. E*, *67*, 026401.
Rädler, K.-H., & Brandenburg, A. 2009, *MNRAS*, *393*, 113.
Rädler, K.-H., Brandenburg, A., Del Sordo, F., & Rheinhardt, M. 2011, *Phys. Rev. E*, *84*, 4.
Rogachevskii, I., Kleeorin, N., Brandenburg, A., & Eichler, D. 2012, *ApJ*, *753*, 6.
Schober, J., Brandenburg, A., Rogachevskii, I., et al. 2017, *ApJ*, to be submitted.
Schrinner, M., Rädler, K.-H., Schmitt, D., et al. 2005, *Astron. Nachr.*, *326*, 245.
Schrinner, M., Rädler, K.-H., Schmitt, D., et al. 2007, *Geophys. Astrophys. Fluid Dyn.*, *101*, 81.
Sur, S., Brandenburg, A., & Subramanian, K. 2008, *MNRAS*, *385*, L15.

How to cite this article: Brandenburg A, Schober J and Rogachevskii I. The contribution of kinetic helicity to turbulent magnetic diffusivity. *Astron. Nachr./AN*. 2017;338:790–793. https://doi.org/10.1002/asna.201713384.